chemengineering

MDPI

Article

Understanding Catalysis—A Simplified Simulation of Catalytic Reactors for CO_2 Reduction

Jasmin Terreni [1,2], Andreas Borgschulte [1,2,*], Magne Hillestad [3] and Bruce D. Patterson [1,4]

1 Laboratory for Advanced Analytical Technologies, Empa, CH-8600 Dübendorf, Switzerland; jasmin.terreni@empa.ch (J.T.); bruce.patterson@bluewin.ch (B.D.P.)
2 Department of Chemistry, University of Zurich, CH-8057 Zurich, Switzerland
3 Department of Chemical Engineering, Norwegian University of Science and Technology (NTNU), N-7491 Trondheim, Norway; magne.hillestad@ntnu.no
4 Department of Physics, University of Zurich, CH-8057 Zurich, Switzerland
* Correspondence: andreas.borgschulte@empa.ch; Tel.: +41-58-765-46-39

Received: 11 August 2020; Accepted: 10 November 2020; Published: 20 November 2020

Abstract: The realistic numerical simulation of chemical processes, such as those occurring in catalytic reactors, is a complex undertaking, requiring knowledge of chemical thermodynamics, multi-component activated rate equations, coupled flows of material and heat, etc. A standard approach is to make use of a process simulation program package. However for a basic understanding, it may be advantageous to sacrifice some realism and to independently reproduce, in essence, the package computations. Here, we set up and numerically solve the basic equations governing the functioning of plug-flow reactors (PFR) and continuously stirred tank reactors (CSTR), and we demonstrate the procedure with simplified cases of the catalytic hydrogenation of carbon dioxide to form the synthetic fuels methanol and methane, each of which involves five chemical species undergoing three coupled chemical reactions. We show how to predict final product concentrations as a function of the catalyst system, reactor parameters, initial reactant concentrations, temperature, and pressure. Further, we use the numerical solutions to verify the "thermodynamic limit" of a PFR and a CSTR, and, for a PFR, to demonstrate the enhanced efficiency obtainable by "looping" and "sorption-enhancement".

Keywords: CO_2 reduction; methanol; methane; thermodynamics; kinetics; reactor design

1. Introduction

Serious catalytic reactor design is a complex task involving the coupled phenomena of chemical thermodynamics, multi-step chemical reactions, hydrodynamic flowand the generation, conduction, and dissipation of heat. Sophisticated computer software packages [1,2] are widely used to aid the reactor designer, but it has been argued that the "black-box" results they provide may obscure fundamental relationships, which are important for a more basic understanding. Quoting Reference [3], "A potential pedagogical drawback to simulation packages such as HYSYS and ASPEN is that it might be possible for students to successfully construct and use models without really understanding the physical phenomena within each unit operation. . . . . Care must be taken to insure that simulation enhances student understanding, rather than providing a crutch to allow them to solve problems with only a surface understanding of the processes they are modeling". Most chemical engineering textbooks [4–9] treat the general principles of catalytic reactor operation in terms of a set of coupled differential equations describing the creation and annihilation of chemical components. These equations are generally highly non-linear, hence requiring numerical techniques for their solution. Textbooks then either treat particularly simple reaction schemes, which do allow analytical solution, or plot numerically

computed results which the average student is unable to reproduce. Only in exceptional cases does a textbook assist the student in generating a suitable computer program to solve non-linear equations [7].

In this work, we demonstrate how one may simulate the simplified operation of a catalytic reactor using basic thermodynamic data, a kinetic model for the multi-step reactions, and numerical solutions of reactor-specific differential equations describing the evolution from reactant to product chemical species. We focus our attention on the two archetypes of continuous-flow reactors: the plug flow reactor (PFR) and the continuously stirred tank reactor (CSTR) [5]. To simplify the discussion, we assume constant and uniform reaction temperature and pressure and we neglect the issues of heat flow and pressure drop. Furthermore, we assume that all reactant and product species behave as ideal gases. In the main text, we explain how the relevant equations are set up to describe the evolution of chemical concentrations in the reactor and we plot and discuss their numerical solutions. Student exercises presented in the Supplementary Materials instruct the reader in the creation of a computer program, based on a variable-step Runge–Kutta integration method [10], to solve non-linear differential equations.

A schematic diagram of the simulation procedure is shown in Figure 1. Once the overall relevant chemical reactions have been defined, basic thermodynamics dictates the Gibbs free energy change and hence the equilibrium constants. From these, the temperature- (T) and pressure- (P) dependent equilibrium state is determined in the thermodynamic limit—i.e., after infinite elapsed reaction time. Dynamic reactor simulation requires knowledge of the concentration-, T-, and P-dependent production rates of the individual chemical species. This information is typically contained in a published "kinetic model", which depends on the catalyst used. Once the reactor type (PFR or CSTR) is defined, coupled differential equations describing the chemical component flows are set up. These equations are then numerically solved to yield the time or position-dependent concentration of each chemical component. A useful check of the computation procedure, including the kinetic model, is to extend the dynamic simulation to infinite elapsed time, which should reproduce the thermodynamic limit obtained earlier.

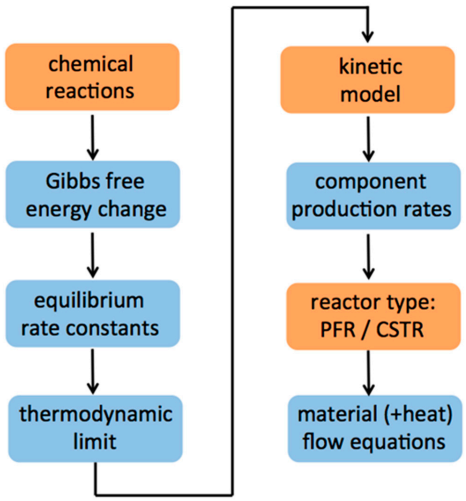

Figure 1. Schematic diagram illustrating the catalytic reactor simulation procedure. Orange boxes indicate the external input of information.

We demonstrate the usefulness of this approach to reactor simulation and hopefully motivate further exploration by the reader by examining the enhanced efficiency of two modifications of the PFR, which effectively shift the thermodynamic equilibrium: product separation and the removal/recycling of unreacted species in a "looped" reactor [7], and product removal by selective absorption ("sorption enhancement") [11]. As mentioned, a series of progressively more challenging student exercises which review and develop the concepts treated in the main text is included, with answers, as an Supplementary Materials.

2. Materials and Methods

Equilibrium constants for the chemical reactions considered were either computed from thermodynamic data on the Gibbs free energy change [12] or taken from the literature [13,14], and the kinetic rate factors were obtained from published models of experimental data [13–15]. The numerical computations were performed with Wolfram Mathematica, Version 11.3 [16].

3. Results and Discussion

3.1. CO_2 Hydrogenation to Methanol and Methane

In order to demonstrate our simulation of catalytic reactors by the setup and numerical solution of kinetic equations, we have chosen as chemical processes the reduction of carbon dioxide by hydrogenation to form the synthetic fuels methanol and methane [17,18]. Note that the production of methane in this fashion is also called "CO_2 methanation". Carbon-based fossil fuels remain the most important energy source worldwide due to the high chemical stability of their combustion product, carbon dioxide [19]. However, carbon dioxide is a major greenhouse gas causing global warming. Therefore viable alternatives to the burning of fossil fuels have to be found, and one option is the use of synthetic carbon-based fuels, produced using renewable energy, and carbon dioxide which has been recycled from natural or industrial processes [17,20]. The CO_2 may then be converted to a fuel by catalytic hydrogenation [18,21,22]. The simplest carbon-based synthetic fuels are the C1 species formic acid (HCOOH), formaldehyde (HCHO), methanol (CH_3OH), and methane (CH_4) (Figure 2). We note that CO_2 can also be converted to higher hydrocarbons and alcohols by Fischer–Tropsch synthesis [18,23].

From Figure 2, we can see that methanol and methane are promising candidates for synthetic carbon-based fuels. Note that the production reactions of both methanol and methane are spontaneous under standard conditions ($\Delta G_{red} < 0$) [24]. While methanol has the advantage of being a liquid at room temperature and hence has a high volumetric energy storage density, the gas methane offers high gravimetric energy storage [25].

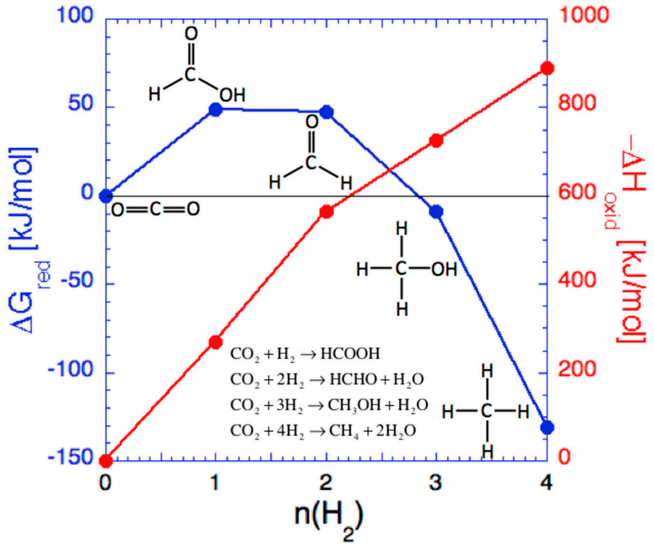

Figure 2. A Latimer–Frost-type diagram [26] showing, as a function of the degree of hydrogen reduction $n(H_2)$ and at standard temperature and pressure, the change in Gibbs free energy ΔG_{red} upon production by CO_2 hydrogenation and the change in enthalpy ΔH_{oxid} upon combustion in oxygen for the C1 chemicals formic acid (HCOOH), formaldehyde (HCHO), methanol (CH_3OH), and methane (CH_4). The negative values of ΔG_{red} for methanol and methane formation imply spontaneous production reactions, and the large values of ΔH_{oxid} imply a high capacity for chemical energy storage. The thermodynamic data are from references [12,27].

The reduction of carbon dioxide to methanol is usually carried out over a copper-zinc oxide catalyst at temperatures of approximately 200–300 °C and a pressure of several tens of bars [13,14,21]. Nickel is a practical catalyst for CO_2 methanation, and the reaction is carried out at a few bars of pressure and temperatures of approximately 250–450 °C [15,21,28,29].

The important overall chemical reactions [14,15] involved in the gas phase hydrogenation of CO_2 to CH_3OH and CH_4 are shown in Figure 3. In both cases, the production can either be direct (reaction 3) or can proceed via carbon monoxide as an intermediate (reactions 2 and 1); the reverse water gas shift (RWGS) reaction 2 competes for CO_2 with direct hydrogenation. From thermodynamic arguments, we can conclude the following: (1) In contrast to the CO_2 and CO hydrogenation reactions, the RWGS reaction 2 is endothermic. Therefore, increasing the reaction temperature will lead to an increase in the formation of CO and will consequently hinder the direct hydrogenation of CO_2 to CH_3OH or CH_4. (2) Since, in both cases, reaction 3 involves a reduction in the number of moles, an increase in pressure will facilitate the direct hydrogenation of CO_2 to CH_3OH or CH_4. These predictions follow from Le Chatelier's principle [24].

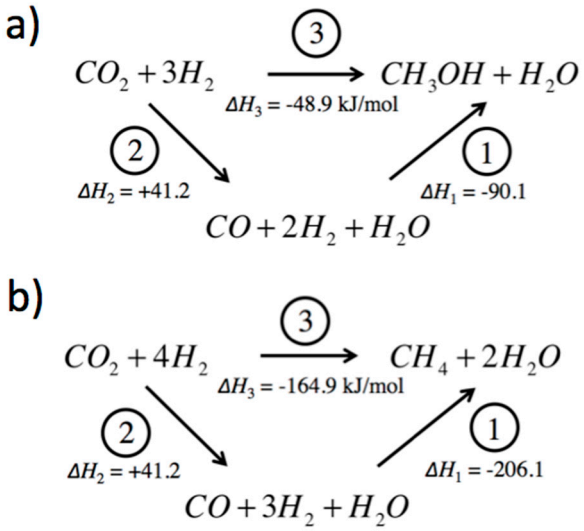

Figure 3. Gas phase CO_2 reduction to methanol (**a**) and methane (**b**) [14,15]. Reaction 3, in each case is the direct hydrogenation of CO_2. Reaction 2 is the reverse water gas shift (RWGS) reaction, and reaction 1 is the hydrogenation of carbon monoxide. Standard enthalpies of formation are from Swaddle [12].

The equilibrium state in the conversion of carbon dioxide to methanol or methane is defined by thermodynamics and can be determined using the temperature-dependent equilibrium constants K^{eq}. These are, in turn, determined by the change in Gibbs free energy at a given temperature [24]. For example, for the direct conversion of CO_2 to CH_3OH in reaction 3 in Figure 3, we have:

$$K_3^{eq}(T) = \exp\left[\frac{-\Delta G_3^0}{RT}\right] = \exp\left[\frac{-\Delta H_3^0 + T\Delta S_3^0}{RT}\right] = exp\left[\frac{-\Delta H^0_{CH_3OH} - \Delta H^0_{H_2O} + 3\Delta H^0_{H_2} + \Delta H^0_{CO_2}}{RT}\right] * exp\left[\frac{S^0_{CH_3OH} + S^0_{H_2O} - 3S^0_{H_2} - S^0_{CO_2}}{R}\right], \quad (1)$$

where T is the absolute temperature, R is the gas constant, and ΔH^0 and S^0 are the standard enthalpy and entropy of formation of the corresponding reactant or product species (Table 1).

Table 1. Standard enthalpy of formation and entropy of involved species for CO_2 reduction to form methanol and methane [12].

	ΔH^0 [kJ/mol]	S^0 [J/mol K]
CO	−110.52	197.67
CO_2	−393.51	213.74
H_2	0	130.68
H_2O	−241.82	188.82
CH_3OH	−200.66	239.81
CH_4	−74.81	186.26

In this way, we arrive at the equilibrium constants for the reactions of Figure 3, as plotted as a function of inverse temperature in Figure 4 for methanol formation (in red) and for methane formation (in blue). The equilibrium constant for the reverse water gas shift reaction (reaction 2) is plotted in green.

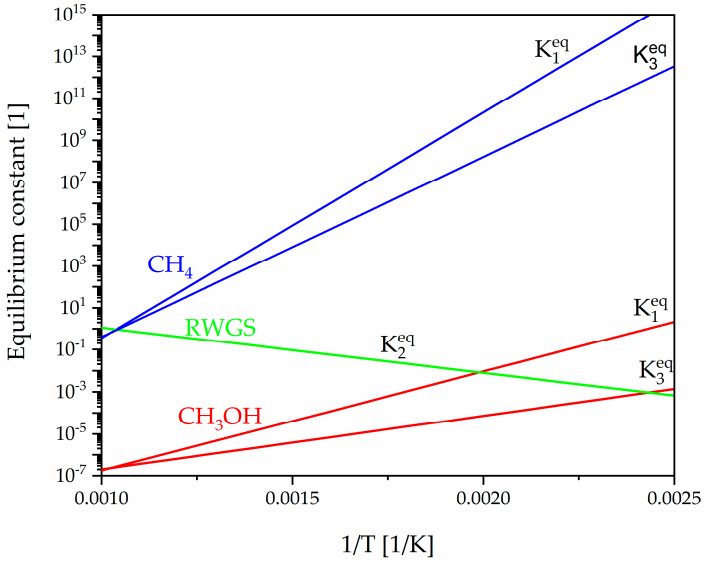

Figure 4. Equilibrium constants for methanol (red) and methane (blue) production reactions as a function of the inverse temperature. The green line shows the equilibrium constant of the reverse water gas shift reaction. Note the substantially higher values for methane production compared to those for methanol and that the endothermic RWGS reaction is enhanced with increasing temperature.

Because the three reactions in each set are coupled, only two of the three equilibrium constants are independent:

$$K_1^{eq}(T) * K_2^{eq}(T) = K_3^{eq}(T). \quad (2)$$

3.2. Thermodynamic Equilibrium

At a given temperature and pressure, the thermodynamic yield of a reaction is the equilibrium result that is approached after an infinite elapsed time. Because of their coupling (Equation (2)), we need only to consider two of the three reactions. The thermodynamic yield is determined by equating the equilibrium constant with the corresponding "reaction quotient" [24]. In the case of methanol synthesis, we consider reactions 2 and 3 of Figure 3 to arrive at the following expressions:

$$K_2^{eq}(T) = \frac{N_{CO} * N_{H_2o}}{N_{H_2} * N_{CO_2}}, \quad (3)$$

$$K_3^{eq}(T) = \frac{N_{CH_3OH} * N_{H_2O} * N_{tot}^2 * P_0^2}{N_{H_2}^3 * N_{CO_2} * P^2}. \quad (4)$$

The reaction quotients are determined by the reduced partial pressures p_j or molar concentrations N_j of the reactant and product species j, the reaction pressure P, and the atmospheric pressure P_0. The molar concentrations, in turn, are related to the degrees of completion ξ_i of the individual reactions i. For the case of methanol synthesis, the relationships between the equilibrium molar concentrations N_j and the degrees of completion ξ_i are given by [30]:

$$N_{CO} = \xi_2 * N_{CO_2}^0, \quad (5)$$

$$N_{CO_2} = (1 - \xi_2 - \xi_3) * N_{CO_2}^0, \quad (6)$$

$$N_{H_2} = (SN + 1 - \xi_2 - 3\xi_3) * N_{CO_2}^0, \quad (7)$$

$$N_{H_2O} = (\xi_2 + \xi_3) * N_{CO_2}^0, \quad (8)$$

$$N_{CH_3OH} = \xi_3 * N_{CO_2}^0, \quad (9)$$

$$N_{tot} = N_{CO} + N_{CO_2} + N_{H_2} + N_{H_2O} + N_{CH_3OH} = (SN + 2 - 2\xi_3) * N_{CO_2}^0. \quad (10)$$

Here, N_{tot} is the total molar concentration and SN is the "stoichiometric number" [31], defined as the ratio between the difference of the initial molar concentrations of hydrogen and carbon dioxide and the sum of the initial concentrations of CO and CO_2:

$$SN = \frac{N_{H_2}^0 - N_{CO_2}^0}{N_{CO}^0 + N_{CO_2}^0}. \quad (11)$$

In the present work, we assume no initial concentration of carbon monoxide ($N_{CO}^0 = 0$). For ideal conditions, $SN = 2$ for CO_2 reduction to methanol and $SN = 3$ for the reduction to methane.

The specification of SN, T, and P allows us to numerically solve Equations (5)–(10) for the two unknowns, ξ_2 and ξ_3, where ξ_3 represents the degree of conversion of CO_2 to CH_3OH. A similar procedure can be applied to treat CO_2 reduction to methane (see Exercises 3–5). The resulting equilibrium conversions for the CO_2 reduction to methanol and methane, with the ideal SN values, are shown as a function of T and P in Figure 5.

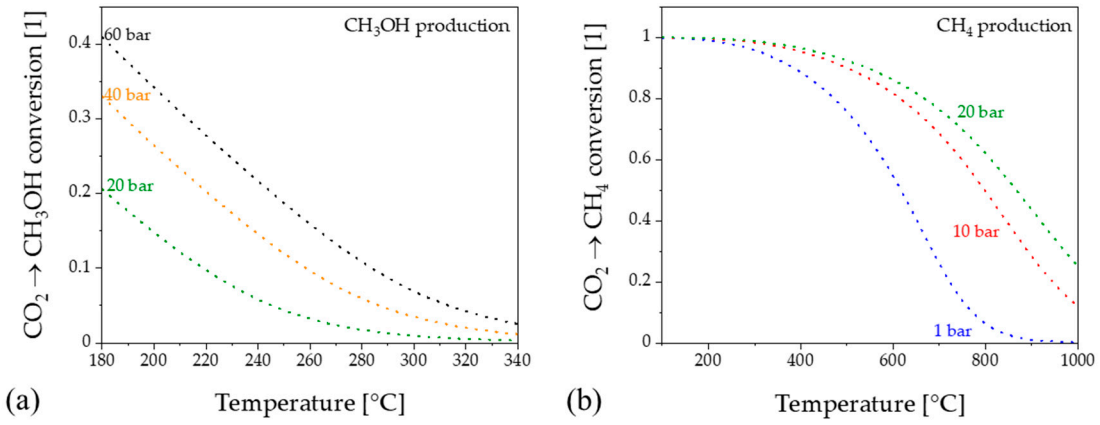

Figure 5. Equilibrium molar conversion for the reduction of CO_2 to methanol (**a**) and to methane (**b**), as a function of temperature and at different pressures.

As predicted by Le Chatelier's principle, the equilibrium conversion of CO_2 to methanol or methane increases with increasing pressure and decreases with increasing temperature. The results in Figure 5 are in good agreement with published studies for methanol [30] and methane [32,33] synthesis.

3.3. Kinetic Behavior in a Continuous Flow Catalytic Reactor

In a practical chemical reactor, a catalyst is used to selectively accelerate the desired reaction. It should be noted that the presence of a catalyst cannot by itself increase the reaction yield beyond that given by thermodynamics; by effectively lowering the pertinent potential energy barrier, it can only increase the rate at which a reaction proceeds [34,35].

A more realistic treatment of a chemical process than that provided by equilibrium thermodynamics requires the analysis of the *kinetic* behavior, which, besides the choice of catalyst, depends on the reactor geometry [4]. In the pharmaceutical industry, a "batch reactor" is often used to repeatedly process limited amounts of material. Here, we consider the kinetic behavior of CO_2 hydrogenation in the two archetypical "continuous flow" reactor types: the "plug flow reactor" (PFR) and the "continuously stirred tank reactor" (CSTR).

The kinetics of the reduction of CO_2 to methanol over a $Cu/ZnO/Al_2O_3$ catalyst have been modeled by Graaf et al. [13,14]. By analyzing the important reaction intermediates and determining the rate-limiting steps, these authors find the following expressions for r_i, the rates of the three reactions in Figure 3a, and hence for **R** a 5-component vector giving the net production rates for the individual chemical species:

$$r_1 = k_1 K_{CO}\left[p_{CO} * p_{H_2}^{\frac{3}{2}} - \frac{p_{CH_3OH}}{P_{H_2}^{\frac{1}{2}} * K_1^{eq}}\right]/denom, \tag{12}$$

$$r_2 = k_2 K_{CO_2}\left[p_{CO_2} * p_{H_2} - \frac{p_{H_2O} * p_{CO}}{K_2^{eq}}\right]/denom, \tag{13}$$

$$r_3 = k_3 K_{CO_2}\left[p_{CO_2} * p_{H_2}^{\frac{3}{2}} - \frac{p_{CH_3OH} * p_{H_2O}}{p_{H_2}^{\frac{3}{2}} * K_3^{eq}}\right]/denom, \tag{14}$$

$$denom = \left(1 + K_{CO} * p_{CO} + K_{co_2} * p_{CO_2}\right) * \left[p_{H_2}^{\frac{1}{2}} + \left(\frac{K_{H_2O}}{K_{H_2}^{\frac{1}{2}}}\right) * p_{H_2O}\right], \tag{15}$$

$$\mathbf{R} = \left(R_{CO}, R_{CO_2}, R_{H_2}, R_{H_2O}, R_{CH_3OH}\right) = (-r_1 + r_2, -r_2 - r_3, -2r_1 - r_2 - 3r_3, r_2 + r_3, r_1 + r_3. \tag{16}$$

Like the equilibrium constants, the temperature-dependent kinetic factors in Equations (12)–(16) also have the Arrhenius form:

$$K_n(T) = a_n * \exp\left(\frac{b_n}{R * T}\right). \tag{17}$$

The values presented by Graaf et al. for the Arrhenius parameters for the various factors in methanol production are given in Table 2. The corresponding factors for methanation are given in Exercise 6 of the Supplementary Materials. Instead of the thermodynamically derived expressions for the equilibrium rate constants $K^{eq}{}_j$, we use for methanol synthesis the expressions from Graaf et al. [13,14] in Table 2.

Table 2. Arrhenius parameters for the temperature-dependent factors in the model of the kinetics of methanol production of Graaf et al. [13,14].

Variable	a	$b\left[\frac{J}{mol}\right]$
K_1^{eq}	2.39×10^{-13}	9.84×10^4
K_2^{eq}	1.07×10^2	-3.91×10^4
K_3^{eq}	2.56×10^{-11}	5.87×10^4
k_1	$4.89 \times 10^7 \frac{mol}{kg\ s}$	-1.13×10^5
k_2	$9.64 \times 10^{11} \frac{mol}{kg\ s}$	-1.53×10^5
k_3	$1.09 \times 10^5 \frac{mol}{kg\ s}$	-0.875×10^5
K_{CO}	2.16×10^{-5}	0.468×10^5
K_{CO_2}	7.05×10^{-7}	0.617×10^5
$K_{H_2O}/K_{H_2}{}^{1/2}$	6.37×10^{-9}	0.840×10^5

3.3.1. Plug Flow Reactor

We first consider the plug flow reactor, where the reactants and products flow with a constant total mass flow rate through one or more parallel tubes filled with loosely packed catalyst. For our calculations, we make the simplifying assumptions: (1) that all reactants and products are ideal gases, and (2) that the temperature and pressure are constant and uniform along the reactor tubes. The working principle and the corresponding method of numerical simulation for the PFR are given in Figure 6. The vector $\dot{\mathbf{N}}$ denotes the molar flow rates (moles/s), the components of which are the x position-dependent flows of CO, CO_2, H_2, H_2O, and CH_3OH. As the gases proceed along the reactor tubes, the initial reactants CO_2 and H_2 are converted to the product species CO, H_2O, and CH_3OH. The values used for the PFR parameters in Figure 6 are shown in Table 3.

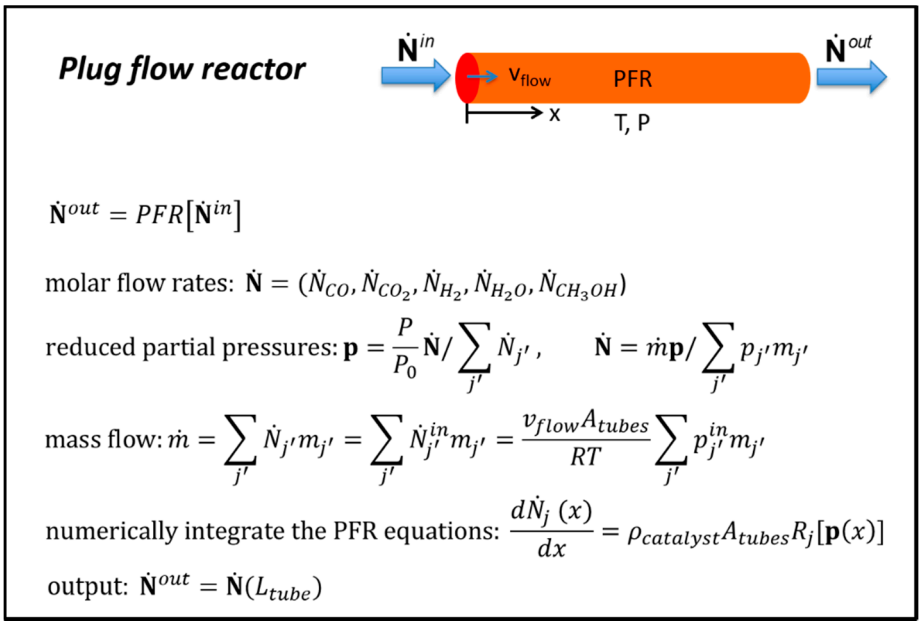

Figure 6. Computational scheme for a plug flow reactor, defining the function *PFR*, which relates the input and output component molar flow rates [5]. The component molecular weights are given by m_j.

Table 3. Plug flow reactor parameter values used in the present simulation of methanol and methane synthesis.

Parameter	Methanol Synthesis	Methane Synthesis
Catalyst	$Cu/ZnO/Al_2O_3$	$Ni/MgAl_2O_4$
Catalyst density $\rho_{catalyst}$	1000 kg/m^3	1000 kg/m^3
Nr of parallel tubes n_{tubes}	10,000	10
Tube diameter d	2 cm	2 cm
Tube area $A_{tube} = n_{tube} \times \pi d^2/4$	3.14 m^2	0.00314 m^2
Tube length L_{tube}	3 m	1 m
Initial flow velocity v_{flow}	0.05 m/s	5 m/s
Stoichiometric number SN	2	3
Temperature range T	180–340 °C	100–1000 °C
Pressures P	20, 40, 60 bar	1, 10, 20 bar

The resulting temperature- and pressure-dependent degree of $CO_2 \rightarrow CH_3OH$ conversion is shown with solid curves in Figure 7 and is in qualitative agreement with previously published studies [36–38]. We highlight two important features: (1) at practical pressures, only a low degree of conversion to methanol (<0.25) is obtained. (2) The conversion predicted by the kinetic behavior cannot exceed the equilibrium value (dotted curves in Figures 5 and 7. We attribute the slight overshoot of the kinetic data at 20 bar to slight inconsistencies in the parameter values of Graaf et al. (Table 2) [13,14].

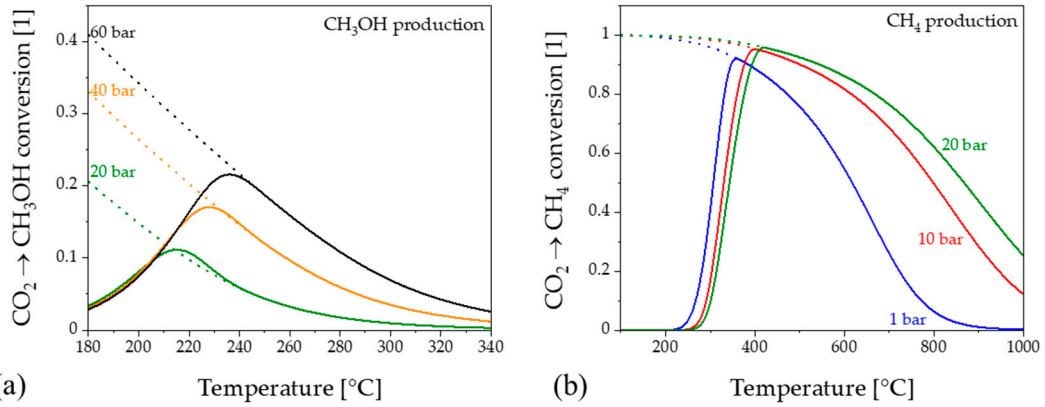

Figure 7. Comparison of the thermodynamic (dotted curves) and kinetic (solid curves) degrees of molar conversion, as a function of temperature and pressure, (**a**) for the reduction of CO_2 to methanol and (**b**) for CO_2 methanation. The assumed values for the reactor parameters are given in Table 3.

We leave as an exercise for the reader the setup of a similar kinetic simulation for CO_2 methanation (Exercises 6–10), using, for example, the kinetic model of Xu and Froment for a $Ni/MgAl_2O_4$ catalyst [15]. We assume an ideal stoichiometric number $SN = 3$, again with no initial CO. As indicated by the equilibrium constants in Figure 4, CO_2 methanation is much more rapid than the reduction of CO_2 to methanol. As a consequence, to obtain the results shown in Figure 7b we have modified the reactor parameter values from the methanol case (see Table 3). Again, our kinetic results are in qualitative agreement with the published data [39].

By taking the tube length L_{tube} to be a variable, one may use the computation scheme of Figure 6 to simulate the molar flow rates of the individual chemical components as a function of position along the reactor tubes (Figure 8). These position dependencies are comparable to those found previously [32,40].

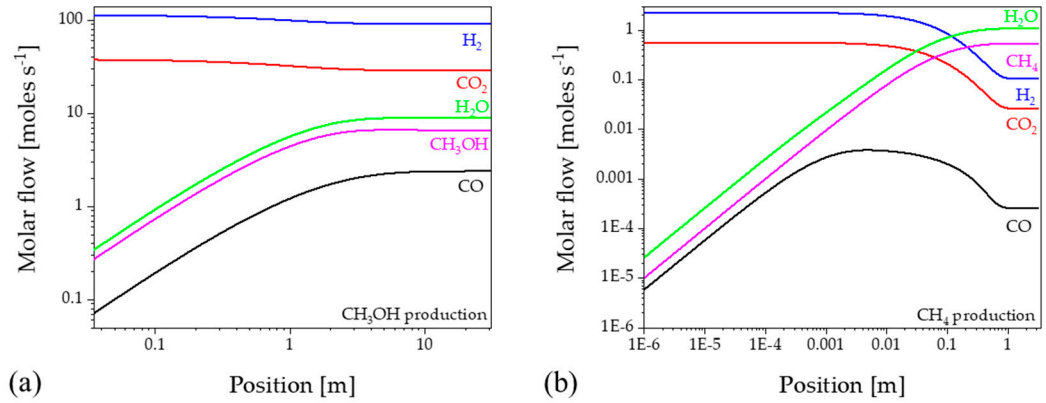

Figure 8. Position-dependent component molar flow rates in a plug flow reactor. (**a**) CO_2 reduction to methanol (40 bar, 230 °C, $SN = 2$); (**b**) CO_2 methanation (10 bar, 400 °C, $SN = 3$).

In Figure 7, we observed that the molar degree of conversion achievable with a simple PFR cannot exceed the value predicted by equilibrium thermodynamics. By greatly extending the length (to impractical sizes), one should, however, approach the thermodynamic limit. In Figure 9, we show the PFR molar conversion for very long PFR tubes, and we confirm the approach to this limit.

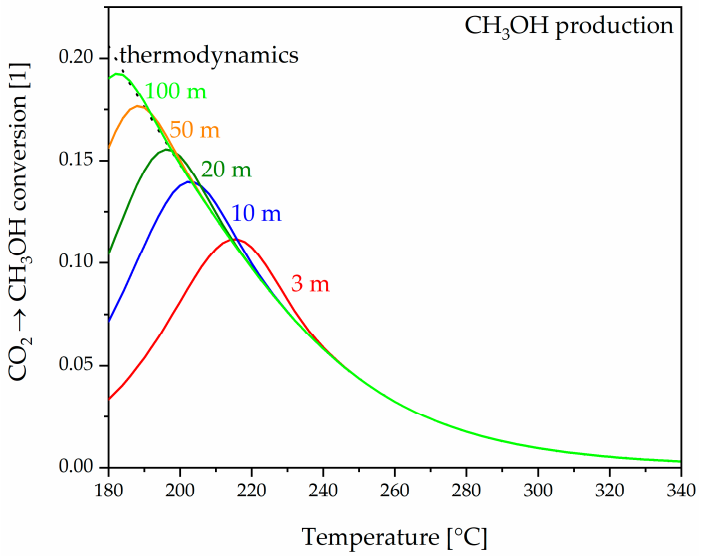

Figure 9. A demonstration that extending the tube length of a plug flow reactor to impractically large sizes causes the degree of molar conversion of CO_2 to CH_3OH to approach the limit given by equilibrium thermodynamics (dotted curves). The pressure is taken to be 20 bar, and the initial stoichiometric number $SN = 2$.

3.3.2. Continuously Stirred Tank Reactor

In an ideal continuously stirred tank reactor (CSTR), the environmental conditions in the reactor are everywhere the same, since the contents (reactants, catalyst, and products) are constantly mixed—e.g., by a mechanical stirrer. The numerical simulation scheme for the CSTR reaction kinetics is given in Figure 10.

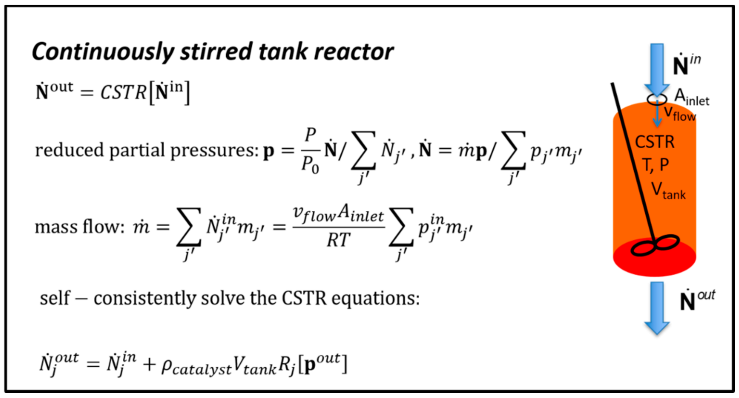

Figure 10. Computational scheme for a continuously stirred tank reactor, defining the function *CSTR*, which relates the input and output component molar flows [5].

The following points provide additional information regarding the computation scheme in Figure 10:

- The volume of the reactor tank is given by V_{tank};
- The reactants enter the tank with a flow velocity v_{flow} through an inlet aperture, the area of which is A_{inlet};
- The remaining variables have the same meaning as for the PFR described in Figure 6;
- The solution of the CSTR equations is self-consistent and requires the component production rates R_j to be evaluated at the exit of the reactor [41].

For calculating the catalytic conversion of CO_2 to CH_3OH in a CSTR, we again use the kinetic model of Graaf et al. [13,14]. In Figure 11, we show the degree of conversion for CO_2 to CH_3OH in a CSTR as a function of temperature and tank volume (V_{tank}). The pressure is constant at 20 bar; the catalyst density is again 1000 kg/m^3; and, as for the methanol PFR case, the initial volumetric flow is taken to be $v_{flow} \times A_{inlet}$ = 3.14 × 0.05 m^3/s. The red curve in Figure 11 corresponds to a CSTR tank volume equal to that of the PFR tubes ($A_{tubes} \times L_{tube}$), with A_{tubes} = 3.14 m^2 and L_{tube} = 3 m. The blue, orange, and green curves correspond to larger tank volumes ($A_{tubes} \times L_{tube}$, with A_{tube} constant but varying L_{tube} = 10, 20, 50, and 100 m, respectively). In analogy with the results of an extra-long PFR reactor (Figure 9), we see from Figure 11 that, with increasing the CSTR tank volume, the degree of CO_2 → CH_3OH conversion increases and approaches the thermodynamic equilibrium value (dotted curve).

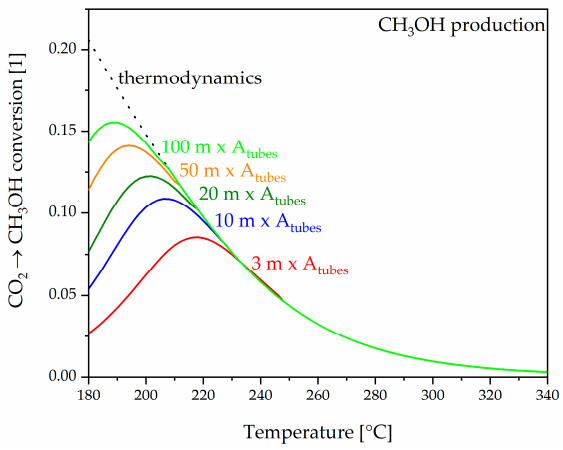

Figure 11. CO_2 → CH_3OH degree of molar conversion for a CSTR (P = 20 bar) as a function of the reactor temperature and tank volume. In analogy with the case for the extra-long PFR (Figure 9), at large values of V_{tank} the CSTR conversion approaches that predicted by equilibrium thermodynamics (dotted curve).

3.4. Modified Plug Flow Reactor

Figure 7 illustrates that the degree of conversion in a PFR, particularly in the case of CO_2 hydrogenation to CH_3OH, is severely limited by thermodynamics. In an attempt to circumvent this limitation, we now simulate two modifications of a PFR—namely, "looping" [7] and "sorption-enhancement" [11]—which have the effect of shifting the thermodynamic equilibrium to allow a more efficient reactor operation. In both cases, this shift of equilibrium is achieved by the continuous removal of reaction products, thus reducing the probability of a back-reaction.

3.4.1. Looped Plug Flow Reactor with Recycling

A well-established method for compensating for the low conversion in methanol synthesis is PFR "looping" [7]. In contrast to a single-pass PFR, a looped PFR recycles the unreacted H_2, CO_2, and CO, as illustrated in the corresponding computation scheme shown in Figure 12.

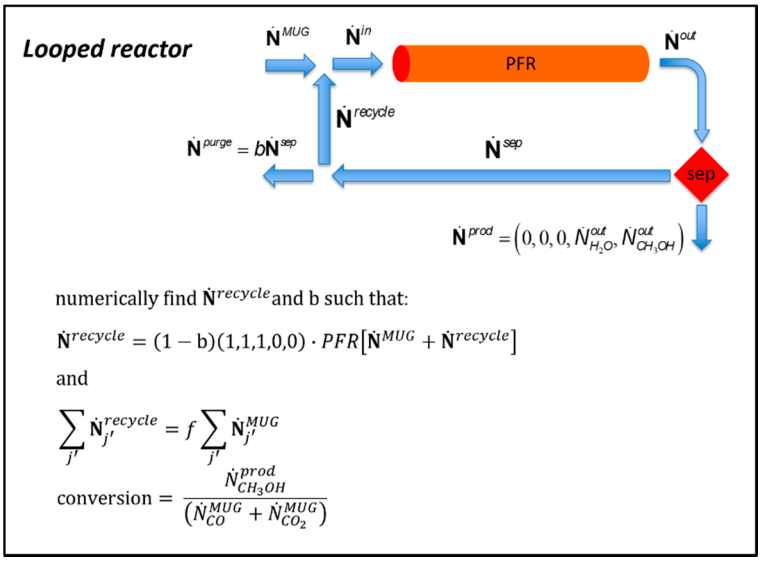

Figure 12. Computational scheme of the looped PFR. The function "*PFR*" refers to the operation of the previously considered single-pass plug flow reactor (Figure 6). The individual molar flows are defined in the Figure.

In the looped PFR, the input "make-up gas" (*MUG*), with a given initial stoichiometric number *SN*, is mixed with the recycled unreacted educt gases prior to entering the PFR. This requires a separation of the reactor output flow, removing the products H_2O and CH_3OH from the unreacted species, CO, CO_2 and H_2, which are then re-introduced at the PFR input. In order to adjust the looping process, a controlled fraction *b* of the recycled gas, principally H_2, is purged. The looping factor *f* effectively determines how many times the unreacted gases are recycled through the reactor. The looping causes an increase in the overall conversion efficiency compared to the single-pass PFR, as shown in Figure 13, where a *MUG* stoichiometric number of $SN = 2.02$ and a looping factor of $f = 4$ are used. The efficiency increase in a looped PFR comes at the expense of the "temperature swing" required to re-heat the recycled unreacted gases following product removal by condensation.

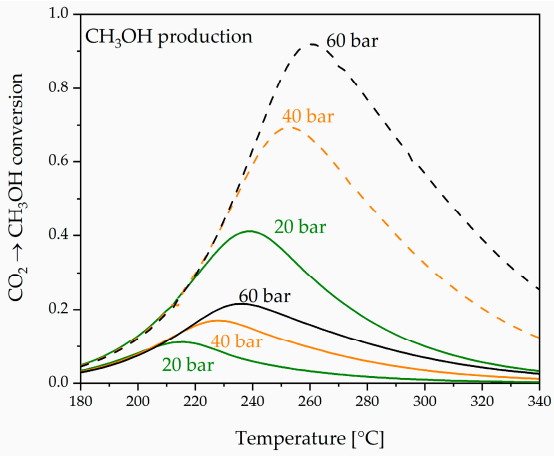

Figure 13. Simulated CO_2 to CH_3OH molar conversion efficiency for a looped PFR (dashed curves), compared to that for a single-pass PFR (solid curves). For the looped PFR, the stoichiometric number *SN* of the incoming make-up gas (*MUG*) is taken to be 2.02 (with no initial CO), and the looping factor f is 4.

3.4.2. Sorption-Enhanced Plug Flow Reactor

A second method of increasing the PFR conversion efficiency is by "sorption enhancement" [11]. The corresponding simulation scheme is shown in Figure 14. Compared to the basic PFR scheme of Figure 6, note the presence of an effective "sorbent channel" and the addition of H_2O and CH_3OH "transfer terms" in the differential PFR equations.

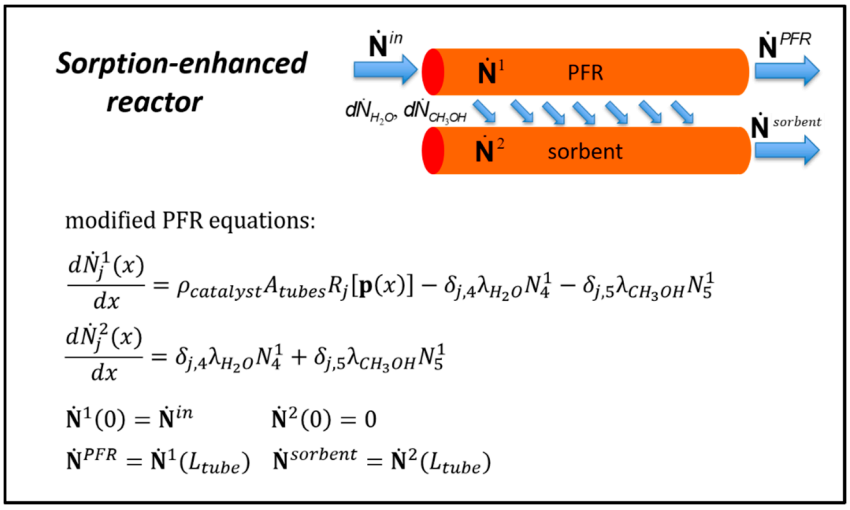

Figure 14. Computational scheme of the sorption-enhanced reactor. Note the presence of a parallel "sorbent" channel and the addition of new H_2O and CH_3OH "transfer" terms to the PFR equations. The symbol δ_{jk} is the "Kronecker delta". The individual molar flows are defined in the figure.

As in the case of the looped PFR, the idea of the sorption-enhanced reactor is that the product is constantly removed from the gas stream by a suitable absorber and, consequently, the equilibrium of the reaction is shifted toward the product side, in accord with Le Chatelier's principle [11]. We can model such a reactor by introducing a second parallel channel, the "sorption channel", and by introducing terms in the PFR equations (those proportional to the inverse transfer lengths λ_k), which cause a continuous transfer of the products H_2O (k = 4) and/or CH_3OH (k = 5) from the PFR channel to the sorption channel. We show the results, in Figure 15, for two cases respectively: (a) $\lambda_{CH_3OH} = 0$—i.e., water absorption only—and (b) $\lambda_{CH_3OH} = \lambda_{H_2O}$—i.e., the simultaneous absorption of both water and methanol. The efficiency enhancement is particularly pronounced when both product species are absorbed. In a practical sorption enhanced PFR, the product absorption occurs in

the catalyst system itself [42]. The sorption-enhanced PFR suffers the drawback of requiring a recurring "pressure-swing", to first desorb from and then to re-pressurize the absorbing catalyst material.

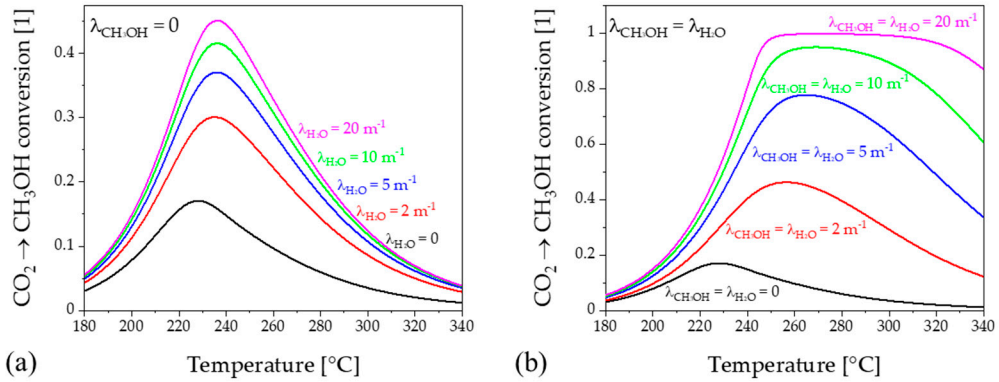

Figure 15. Simulated sorption-enhanced PFR conversion of CO_2 to CH_3OH: (**a**) Water adsorption alone, with methanol extraction from channel 1. (**b**) Simultaneous adsorption of water and methanol, with methanol extraction from channel 2. In both cases, the pressure is 40 bar, and the stoichiometric factor $SN = 2$.

4. Summary and Conclusions

This work has presented, in tutorial form, recipes for the numerical simulation of catalytic reactions. The application examples chosen are the hydrogenation reduction of carbon dioxide to form the synthetic fuels methanol and methane, and it has been assumed throughout that the reactants and products are ideal gases and that the reactor temperature and pressure are constant and uniform. Based on the change in the standard Gibbs free energy, the degrees of chemical conversion were first calculated in thermodynamic equilibrium. The results are in good agreement with the qualitative predictions of Le Chatelier's principle. In a practical chemical reactor, a catalyst is used to selectively accelerate the reaction rate. The dynamic behaviors of the two archetypical continuous-flow reactors, the plug flow reactor (PFR) and the continuously stirred tank reactor (CSTR), were simulated by incorporating published models for the catalyst-specific, multi-step chemical kinetics into reactor-specific differential equations for the product yield. The numerical solution of these equations quantified the effects on the reaction yield of temperature, pressure, and various reactor parameters, in reasonable agreement with previous published work. In particular, it could be shown that, for a very long PFR or a very large volume CSTR, we regain the thermodynamic limit. It was also shown how the evolution from reactant to product species may be spatially followed along the length of the PFR tubes. The thermodynamic limit, in particular the low efficiency of methanol production, can be influenced by shifting the chemical equilibrium—e.g., via the continuous removal of product species. Using our numerical framework, it was demonstrated how this can facilitate methanol production for two particular cases: PFR looping (product removal and reactant recycling—involving a continuous "temperature-swing") and sorption-enhanced PFR (product removal via absorption, perhaps on a specialized catalyst—involving repeated "pressure-swings").

All of these simulations could have been performed using a commercial software package. By laying out the fundamental concepts and constructing and solving the reactor-specific differential equations for the chemical yield, we have attempted to provide the reader with a view into the inner workings of such a "black-box" package. The student exercises in the Supplementary Materials lead the reader through the creation of a homemade computer program to numerically solve the differential equations. Our hope is that our audience will gain an understanding of the basic principles governing catalytic reactors and will be motivated to apply and adapt the presented formalism to applications of specific interest.

Supplementary Materials: The following are available online at http://www.mdpi.com/2305-7084/4/4/62/s1: see Supporting Information with exercises.

Author Contributions: Conceptualization: J.T. and B.D.P.; Formal analysis: J.T., A.B., M.H., B.D.P.; Investigation: J.T. and B.D.P.; Supervision: B.D.P.; Writing—original draft: J.T. and B.D.P.; Writing—review and editing: J.T., A.B., M.H., B.D.P. All authors have read and agreed to the published version of the manuscript.

Funding: This work was partly supported by the UZH-UFSP program LightCheC. The financial support from BFE and FOGA (SmartCat Project) and the Swiss National Science Foundation (Grant no. 200021_144120 and 172662) is acknowledged.

Conflicts of Interest: The authors declare no conflict of interest.

References

1. Tripodi, A.; Compagnoni, M.; Martinazzo, R.; Ramis, G.; Rossetti, I. Process simulation for the design and scale up of heterogeneous catalytic process: Kinetic modeling issues. *Catalysis* **2017**, *7*, 159. [CrossRef]
2. Haydary, J. *Chemical Process Design and Simulation: Aspen Plus and Aspen HYSYS Applications*; John Wiley & Sons, Inc.: Hoboken, NJ, USA, 2019.
3. Savelski, M.J.; Hesketh, R.P. Issues encountered with students using process simulators. *Age* **2002**, *8*, 1.
4. Fogler, S.H. *Elements of Chemical Reaction Engineering*; Pearson Education Inc.: Upper Saddle River, NJ, USA, 1987.
5. Davis, M.E.; Davis, R.J. *Fundamentals of Chemical Reaction Engineering*; McGraw Hill: New York, NY, USA, 2003.
6. Manos, G. Introduction to Chemical Reaction Engineering. In *Concepts of Chemical Engineering 4 Chemists*; Simons, S., Ed.; The Royal Society of Chemistry: Cambridge, UK, 2007.
7. Nauman, E.B. *Chemical Reactor Design, Optimization, and Scaleup*; John Wiley & Sons: Hoboken, NJ, USA, 2007.
8. Hill, C.G.; Root, T.W. *Introduction to Chemical Engineering Kinetics and Reactor Design*; John Wiley & Sons, Inc.: Hoboken, NJ, USA, 2014.
9. Hagen, J. *Industrial Catalysis*; WILEY-VCH Verlag GmbH & Co. KGaA: Weinheim, Germany, 2015.
10. Press, W.H.; Flannery, B.P.; Teukolsky, S.A.; Vetterling, W.T. *Numerical Recipes: The Art of Scientific Computing*; Cambridge University Press: Cambridge, UK, 2007.
11. Carvill, B.T.; Hufton, J.R.; Anand, M.; Sircar, S. Sorption-Enhanced Reaction Process. *AIChE J.* **1996**, *42*, 2765–2772. [CrossRef]
12. Swaddle, T.W. *Inorganic Chemistry—An Industrial and Environmental Perspective*; Academic Press: Cambridge, MA, USA, 1997.
13. Graaf, G.H.; Stamhuis, E.J.; Beenackers, A.A.C.M. Kinetics of low-pressure Methanol Synthesis. *Chem. Eng. Sci.* **1988**, *43*, 3185–3195. [CrossRef]
14. Graaf, G.H.; Scholtens, H.; Stamhuis, E.J.; Beenackers, A.A.C.M. Intra-particle Diffusion Limitations in low-pressure Methanol Synthesis. *Chem. Eng. Sci.* **1990**, *45*, 773–783. [CrossRef]
15. Xu, J.; Froment, G.F. Methane Steam Reforming, Methanation and Water-gas Shift: I. Intrinsic Kinetics. *AlChE J.* **1989**, *35*, 88–96. [CrossRef]
16. Wolfram, S. *Mathematica: A System for Doing Mathematics by Computer*; Addison-Wesley: Reading, MA, USA, 1991.
17. Centi, G.; Quadrelli, E.A.; Perathoner, S. Catalysis for CO_2 conversion: A key technology for rapid introduction of renewable energy in the value chain of chemical industries. *Energy Environ. Sci.* **2003**, *6*, 1711. [CrossRef]
18. Wang, W.; Wang, S.; Ma, X.; Gong, J. Recent advances in catalytic hydrogenation of carbon dioxide. *Chem. Soc. Rev.* **2011**, *40*, 3703–3727. [CrossRef]
19. Abas, N.; Kalair, A.; Khan, N. Review of fossil fuels and future energy technologies. *Futures* **2015**, *69*, 31–49. [CrossRef]
20. Patterson, B.D.; Mo, F.; Borgschulte, A.; Hillestad, M.; Joos, F.; Kristiansen, T.; Sunde, S.; van Bokhoven, J.A. Renewable CO_2 recycling and synthetic fuel production in a marine environment. *Proc. Natl. Acad. Sci. USA* **2019**, *116*, 12212–12219. [CrossRef]
21. Miguel, C.V.; Soria, M.A.; Mendes, A.; Madeira, L.M. Direct CO_2 hydrogenation to methane or methanol from post-combustion exhaust streams—A thermodynamic study. *J. Nat. Gas Sci. Eng.* **2015**, *22*, 1–8. [CrossRef]
22. Porosoff, M.D.; Yan, B.; Chen, J.G. Catalytic reduction of CO_2 by H_2 for synthesis of CO, methanol and hydrocarbons: Challenges and opportunities. *Energy Environ. Sci.* **2016**, *9*, 62. [CrossRef]

23. Moioli, E.; Mutschler, R.; Züttel, A. Renewable energy storage via CO_2 and H_2 conversion to methane and methanol: Assessment for small scale applications. *Renew. Sustain. Energy Rev.* **2019**, *107*, 497–506.
24. Atkins, P.W.; de Paula, J. *Physikalische Chemie*; Wiley-VCH Verlag GmbH & Co. KGaA: Weinheim, Germany, 2006.
25. Schüth, F. Chemical Compounds for Energy Storage. *Chem. Ing. Tech.* **2011**, *83*, 1984–1993. [CrossRef]
26. Koppenol, W.H.; Rush, J.D. Reduction potential of the carbon dioxide/carbon dioxide radical anion: A comparison with other C1 radicals. *J. Phys. Chem.* **1987**, *91*, 4429–4430. [CrossRef]
27. Rumble, J. *CRC Handbook of Chemistry and Physics*; Taylor & Francis: Abdingdon, UK, 2020.
28. Aziz, M.A.A.; Jalil, A.A.; Triwahyono, S.; Ahmad, A. CO_2 methanation over heterogeneous catalysts: Recent progress and future prospects. *Green Chem.* **2015**, *17*, 2647–2663. [CrossRef]
29. Kustov, A.L.; Frey, A.M.; Larsen, K.E.; Johannessen, T.; Nørskov, J.K.; Christensen, C.H. CO methanation over supported bimetallic Ni-Fe catalysts: From computational studies towards catalyst optimization. *Appl. Catal. A Gen.* **2007**, *320*, 98–104. [CrossRef]
30. Skrzypek, J.; Lachowska, M.; Serafin, D. Methanol Synthesis from CO_2 and H_2: Dependence of equilibrium conversions and exit equilibrium concentrations of components on the main process variables. *Chem. Eng. Sci.* **1990**, *45*, 89–96. [CrossRef]
31. Stangeland, K.; Li, H.; Yu, Z. Thermodynamic analysis of chemical and phase equilibria in CO_2 hydrogenation to methanol, dimethyl ether, and higher alcohols. *Ind. Eng. Chem. Res.* **2018**, *57*, 4081–4094. [CrossRef]
32. Schlereth, D.; Hinrichsen, O. A fixed-bed reactor modeling study on the methanation of CO_2. *Chem. Eng. Res. Des.* **2014**, *92*, 702–712.
33. Rönsch, S.; Schneider, J.; Matthischke, S.; Schlüter, M.; Götz, M.; Lefebvre, J.; Prabhakaran, P.; Bajohr, S. Review on methanation—From fundamentals to current projects. *Fuel* **2016**, *166*, 276–296.
34. Hanefeld, U.; Lefferts, L. *Catalysis: An Integrated Textbook for Students*; John Wiley & Sons: Hoboken, NJ, USA, 2018.
35. Nørskov, J.K.; Studt, F.; Abild-Pedersen, F.; Bligaard, T. *Fundamental Concepts in Heterogeneous Catalysis*; John Wiley & Sons, Inc.: Hoboken, NJ, USA, 2014.
36. Toyir, J.; Miloua, R.; Elkadri, N.E.; Nawdali, M.; Toufik, H.; Miloua, F.; Saito, M. Sustainable process for the production of methanol from CO_2 and H_2 using Cu/ZnO-based multicomponent catalyst. *Phys. Procedia* **2009**, *2*, 1075–1079. [CrossRef]
37. Gaikwad, R.; Bansode, A.; Urakawa, A. High-pressure advantages in stoichiometric hydrogenation of carbon dioxide to methanol. *J. Catal.* **2016**, *343*, 127–132.
38. Slotboom, Y.; Bos, M.J.; Pieper, J.; Vrieswijk, V.; Likozar, B.; Kersten, S.R.A.; Brilman, D.W.F. Critical assessment of steady-state kinetic models for the synthesis of methanol over an industrial $Cu/ZnO/Al_2O_3$ catalyst. *Chem. Eng. J.* **2020**, *389*, 124181.
39. Cao, H.; Wang, W.; Cui, T.; Zhu, G.; Ren, X. Enhancing CO_2 hydrogenation to methane by Ni-based catalyst with V species using 3D-mesoporous KIT-6 as support. *Energies* **2020**, *13*, 2235. [CrossRef]
40. Van-Dal, E.S.; Bouallou, C. Design and simulation of a methonal production plant from CO_2 hydrogenation. *J. Clean. Prod.* **2013**, *57*, 38–45.
41. Falconer, J.L. Comparing CSTR and PFR Mass Balances, LearnChemE Video Presentation, Univ. Colorado, Boulder, and Private Communication. 2019. Available online: www.youtube.com/watch?v=xrOdRKzlkcE (accessed on 15 November 2020).
42. Terreni, J.; Trottmann, M.; Franken, T.; Heel, A.; Borgschulte, A. Sorption-Enhanced Methanol Synthesis. *Energy Technol.* **2019**, *7*, 1801093. [CrossRef]